

A new class of axion haloscope resonators: the polygonal coaxial cavity

R. Di Vora,* A. Lombardi, A. Ortolan, and G. Ruoso
INFN, Laboratori Nazionali di Legnaro, Legnaro, Padova, Italy

C. Braggio
*Dipartimento di Fisica e Astronomia, Padova, Italy and
INFN, Sezione di Padova, Padova, Italy*

G. Carugno and A. Gardikiotis
INFN, Sezione di Padova, Padova, Italy
(Dated: March 22, 2024)

In the search for axionic Dark Matter, the high frequency part of the QCD axion parameter space is favored, as indicated by both cosmological and astrophysical arguments and recent indications from lattice QCD calculations. To extend the probing range of cavity haloscopes, solutions addressing the unfavorable scaling of cavity volume with frequency must be developed. Here, we present a novel type of high-volume thin shell resonator for high frequency haloscope dark matter searches. The cavity is formed by two nested and coaxial right angle polygonal prisms enclosed within two flat endcaps. For the axion-sensitive (pseudo-)TM010 mode, finite element simulations yield form factor of the order of 0.8 and Q factor of the order of 60000 for a copper cavity at 4 K. High tunability of up to $\sim 5\%$ is achieved by reciprocal rotation of the two prisms, without significant changes in haloscope sensitivity. A prototype aluminium hexagonal cavity was built and tested, confirming the main characteristics of the design.

I. INTRODUCTION

The axion is a pseudo-Goldstone boson introduced by Weinberg [1] and Wilczek [2] as part of the Peccei-Quinn mechanism to solve the Standard Model puzzle known as the strong-CP problem of Quantum Chromodynamics (QCD) [3, 4]. In current axion models, the QCD axion would have low mass and very weak interaction with ordinary matter. Additionally, cosmological axions created during the Peccei-Quinn phase transition would be non-relativistic and have decay times much longer than the age of the universe, making such 'invisible' axions ideal candidates for the composition of Dark Matter. Astrophysical bounds and cosmological considerations select a range of $1 \mu\text{eV} < m_a < 10 \text{meV}$ [5, 6], with recent lattice QCD calculations favoring the 40-180 μeV region [7].

In the last few years, increasing efforts have been invested into the detection of the axion as the possible majority constituent of Cold Dark Matter, with a large portion of the experiments employing the axion haloscope originally proposed by P. Sikivie [8]. In its simplest form, this experimental scheme exploits the large temporal (and spatial) coherence of the axion field by collecting the power released in a microwave resonator immersed in a strong magnetic field. The converted axion power is (in the limit $Q_0 \ll Q_a$):

$$P_a = g_{a\gamma\gamma}^2 \frac{\rho_a}{m_a^2} \omega_c B_0^2 C V Q_0 \frac{\beta}{(1 + \beta)^2}, \quad (1)$$

where $g_{a\gamma\gamma}$ is the axion to photon effective coupling, $\rho_a \sim 0.45 \text{GeV}/\text{cm}^3$ is the axion density [6], m_a is the axion mass, ω_c is the cavity frequency, B_0 the employed static magnetic field, Q_0 is the unloaded quality factor of the cavity mode, and β is the coupling coefficient of the antenna to the cavity mode.

The form factor C expresses the overlap between the electric field $\mathbf{E}_{\text{mnl}}(\vec{x})$ of the employed cavity mode and the external magnetic field $\mathbf{B}(\vec{x})$ enabling the axion-to-photon conversion. It is given by

$$C = \frac{|\int_V \mathbf{E}_{\text{mnl}} \cdot \mathbf{B} d^3x|^2}{\int_V |\mathbf{B}|^2 d^3x \int_V \epsilon |\mathbf{E}_{\text{mnl}}|^2 d^3x}, \quad (2)$$

where $\epsilon(\vec{x})$ is the dielectric constant at every point \vec{x} in the cavity volume V . In the following we will assume $\mathbf{B}(\vec{x}) = B_0 \hat{\mathbf{z}}$.

Since the axion frequency is to date unknown, an axion haloscope must be able to tune its resonator to cover a range of frequencies. The speed at which this range can be scanned at a certain level of sensitivity in $g_{a\gamma\gamma}$ is called the haloscope scan rate [9]. It is directly proportional to the so-called 'figure of merit' F , which collects all the cavity-related parameters

$$F = (CV)^2 Q_0, \quad (3)$$

the most useful quantity in the design of a new cavity.

Solenoids are the common source of strong intensity magnetic fields. For a given coil length, the available volume scales with the square radius of the bore. Assuming the use of a cylindrical empty cavity as the resonator, the figure of merit is maximized by its fundamental mode

* The authors to whom correspondence may be addressed:
divora@lnl.infn.it

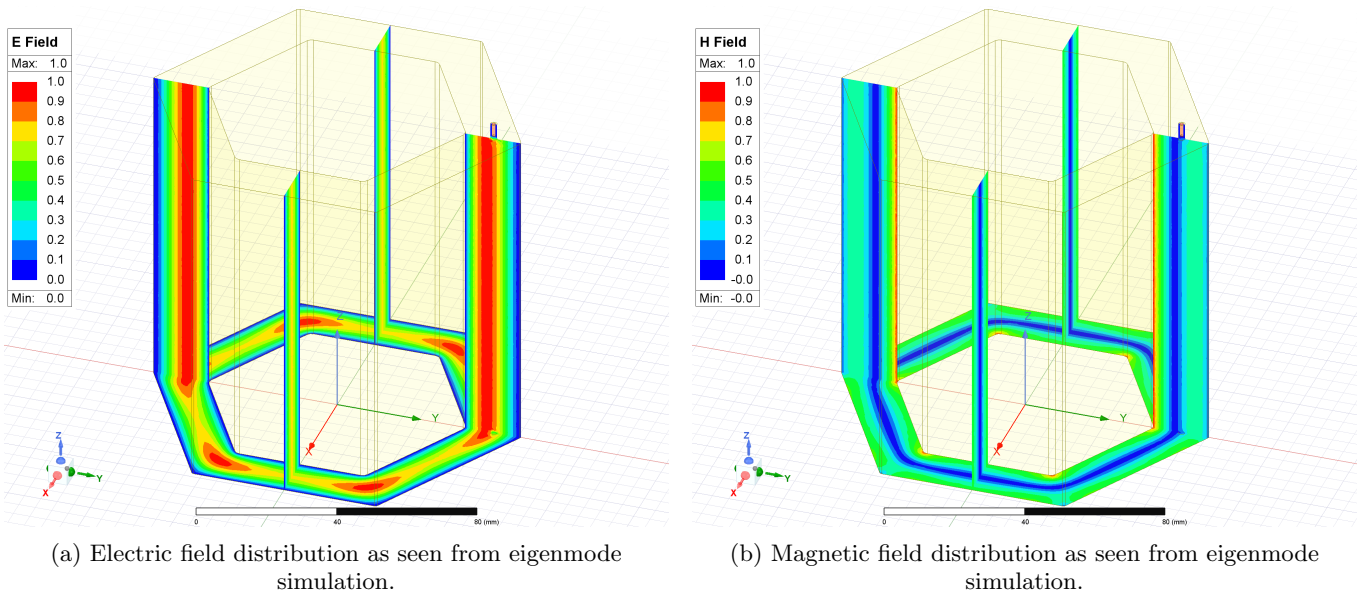


FIG. 1: Basic cavity model used for simulation studies. The cavity is an empty region delimited by two solid copper coaxial polygonal prisms and two endcaps. Each endcap hosts a coax port used for modal simulations. The auxiliary copper structure enveloping the cavity is not shown in the figure.

TM_{010} , whose resonant frequency is set by the inverse of the diameter of the cavity. An increase in the targeted mass then automatically results in a quadratic reduction of the volume of the cavity. The haloscope approach is then extremely effective towards the lower end of the QCD axion mass search range, with the most sensitive experiments having already been able to probe the theoretically expected couplings[10, 11].

To address the unfavorable scaling of the signal towards high frequencies, several solutions were put forth to increase the occupation of the magnet bore. Among them, tunable multirod cavities [12, 13], dielectric cavities [14–20], photonic band gap cavities (the so-called “plasma haloscope”) [21–23], the so-called “pizza cavity” or multi-cell concepts [24–26], and the use of an array of K cavities [27–31]. The latter solution is particularly advantageous when the cavities are coherently readout, as the sensitivity gain is proportional to K , instead of just \sqrt{K} as is the case of incoherent arrays [30–32]. However, exploiting coherence becomes increasingly difficult with the number of cavities due to the high accuracy requirements of the mechanical tuning system. The pizza cavity concept instead relies on a single cylindrical cavity filling the available bore, where identical azimuthal slices are separated through conductive diaphragms. This approach, while interesting to maximize the effective volume, leads to a rapid increase of the number of partitions for larger magnet bore radius, further complicating the tuning system. Recently, a new approach has emerged in the form of folded thin shell cavities [33–35], where a large volume is obtained by folding a sheet-like cavity along one of the dimensions. This solution also allows for very wide tuning by a very precise variation of the

shells separation.

In this work we introduce a new, widely- and easily-tunable high-volume resonator for high frequency DM haloscopes. It is based on two nested, polygonal coaxial prisms enclosed within two flat endcaps. This design represents a decisive improvement on the standard TM_{010} empty cylindrical cavity paradigm and exploits what we think is the most simple and robust tuning system possible, i.e. the rigid rotation around a single, fixed axis.

In Sec. II, we describe the cavity design and its fundamental characteristics. Sec. II A details the results of the simulation evaluating the cavity tuning range and the stability of the cavity parameters over this range. We show that as a consequence of the tradeoff between tuning range and effective volume, once operational frequency and external diameter are chosen, there exists an optimal choice of cavity design for each desired tuning range. In Sec. II B we present the results of indicative studies on the influence on the cavity parameters of non-idealities in the cavity geometry, leading to the determination of the maximum allowable tolerances. Experimental results obtained for a full-scale prototype of the cavity are detailed in Sec. III. In Sec. IV the projected sensitivity of the studied approach is then compared to the benchmarks provided by pizza cavities and cavity arrays. Finally, in Sec. V we briefly recap the obtained results and draw our conclusions.

II. THE TUNABLE POLYGONAL RESONATOR

In designing the cavity subject of this work, we first considered a thin shell cavity delimited by two nested

coaxial and concentric cylinders of equal height and flat endcaps. The radii of the two cylinders are r_{in} and r_{ext} respectively (with $r_{\text{in}} < r_{\text{ext}}$). Given the cavity length L , we choose a gap $d = r_{\text{ext}} - r_{\text{in}} \ll \{L, r_{\text{in}}\}$. The properties of such a cavity are easily derived in the limit of large inner radius and infinite sides, where it simplifies to an infinite rectangular box. The gap d sets the frequency of the TM_{010} mode of such a cavity, which has a very high form factor of ~ 0.81 , as reported in [33]. The TM_{010} mode of the cylindrical design maintains azimuthal and longitudinal uniform radial field profiles, thus C and Q values close to those of the TM_{010} mode of the aforementioned limit cavity are expected. Since the volume of such a cavity scales as $\lambda \cdot (r_{\text{in}} + r_{\text{ext}})/2$ instead of λ^2 , it represents an extremely sensitive transducer for QCD axions especially in the high frequency region of the parameter space, where typically available solenoids are much wider than λ .

To use this cavity in a haloscope frequency tuning is necessary. Insertion of conductor or dielectric rods [36] inside the cavity quickly degrades the form factor of the mode, as do any geometrical perturbations that break the cylindrical symmetry of the cavity. The optimal solution is a uniform tuning of the gap width, similarly to what is done in thin shell cavities, but achieving this in a cylindrical geometry appears challenging. However, by substituting the cylinders with right prisms based on regular polygons with the same number of sides, the continuous azimuthal symmetry of the system becomes discrete. Thanks to this symmetry breaking, the azimuthal field distributions and resonant frequency of the transverse modes depend on the reciprocal angle between the two prisms. By simply rotating one prism with respect to the other, we can tune the cavity resonant frequency without excessively impacting the quality factor and the form factor of the mode.

For the present cavity design, the two nested coaxial prisms are enclosed within two flat endcaps. The cavity supports a (pseudo-) TM_{010} axion-sensitive mode between the two prisms as depicted in Fig. 1, where electric and magnetic field distributions are shown. As the cavity has constant section, the field distributions are longitudinally uniform.

A. Cavity Frequency Tuning

By using a finite element simulation (FEM) software package (Ansys HFSS) we study the properties of our resonator. In the cavity model we choose internal and external circumradiuses or $r_{\text{in}} = 39.14$ mm and $r_{\text{ext}} = 55.92$ mm respectively. The gap width d sets at first order the resonant frequency, while the number of sides determines the obtainable tuning range. We define an angle ϕ to describe the relative rotation of the two prisms, setting $\phi = 0$ when the prisms have parallel sides. Due to symmetry and cyclicity of the system, ϕ values span the range 0 to $\phi_{\text{max}} = \pi/N$. Fig. 2 shows the electric field profiles

obtained from FEM simulations for different rotation angles. The rotation concentrates the electric field at the external prism vertexes, increasing the effective width of the cavity and in turn diminishing the cavity frequency.

In Fig. 3 we plot the cavity parameters for polygonal resonators with $N = 5$ to 9 sides, as a function of ϕ/ϕ_{max} .

To reduce computational costs we used 50 mm-length cavities with the same circumradii as in Fig. 2. Despite the relatively short cavity length, the quality factor Q_0 is dominated by dissipation on the lateral faces. As the cavity wall gap changes with number of sides, the values of the resonant frequency f_0 of the TM_{010} mode at $\phi = 0$ are reported in Tab. I.

TABLE I: Resonant frequency at $\phi = 0$ for different sides numbers.

| Side number | 5 | 6 | 7 | 8 | 9 |
|-------------|--------|--------|-------|-------|-------|
| f_0 (GHz) | 10.820 | 10.165 | 9.798 | 9.574 | 9.425 |

The change of the normalized frequency f/f_0 with ϕ is larger for smaller numbers of sides, as is the case for Q_0 , which increases up to 30% at maximum tuning. This is related to the concentration of the field towards the vertexes: at angles different from 0, the gap between external vertex and the face of the inner polygon increases for smaller sides number, while the opposite holds for the gap between the midpoint of the external faces and the inner vertexes. This in turn leads to increased mode confinement, greater frequency shifts and to smaller surfaces for the mode currents to dissipate on.

In the C factor plot we also include the results of driven modal simulations, which calculate modal S-parameters and field profiles inside the cavity by driving the system through a lumped/wave port. Owing to electromagnetism's reciprocity, the driven modal approach allows for reliable C factor calculation in multi-cell systems. In the present polygonal cavity, C factor estimations via eigenmode simulation, although correct for the initial cavity configuration, could give incorrect results once the tuning angle is increased. In fact, the polygonal resonator can be seen as a cyclic concatenation of identical cavities or cells, and the overall system behaviour depends on the coupling strength between adjacent cells. While in the case of strong coupling the system behaves as a single cavity, for couplings smaller than the mode linewidth the energy deposited in a cell will mostly be dissipated on its walls instead of being transmitted to the neighboring ones. As a consequence, for couplings close to or smaller than the mode linewidth, the eigenmode simulation yields a C factor much higher than the real one. The latter effectively mimics the axion signal being equally transduced into each cell but fails to model the pickup of the signal from a single one [37].

Mode crossings, i.e. regions where the axion-sensitive mode mixes with intruder modes, have been studied using driven modal simulations in the $N = 6$ case. The

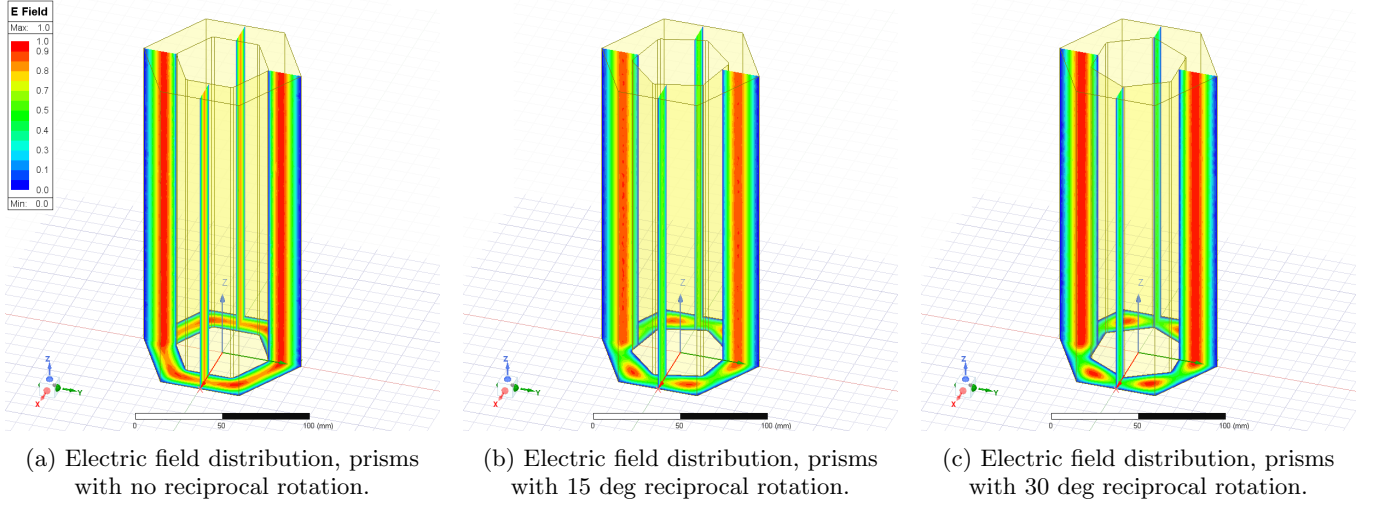


FIG. 2: Electric field profiles obtained from HFSS eigenmode simulation for the TM_{010} mode. Cavity dimensions were $r_{in} = 39.14$ mm and $r_{ext} = 55.92$ mm for the internal and external circumradii and $L = 210$ mm for the length.

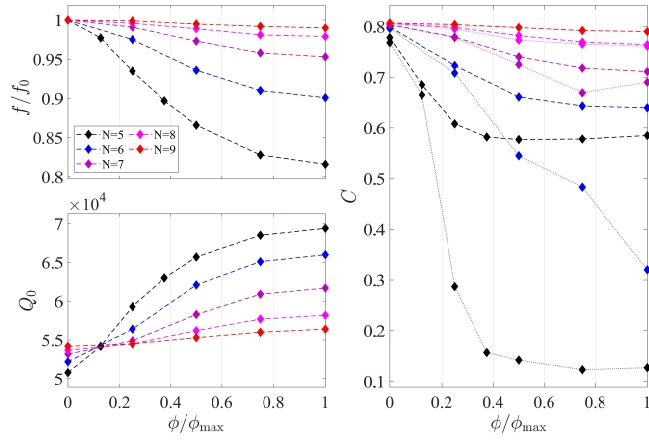


FIG. 3: Internal prism rotation and cavity parameters for different sides number. Left: normalized frequency shift and unloaded quality factor. Right: form factor. Results obtained with eigenmode simulations are plotted with dashed lines, while dotted lines indicate results obtained using driven modal simulations. Compared to the model shown in Fig. 2, we use a 50 mm-long cavity to reduce computational costs.

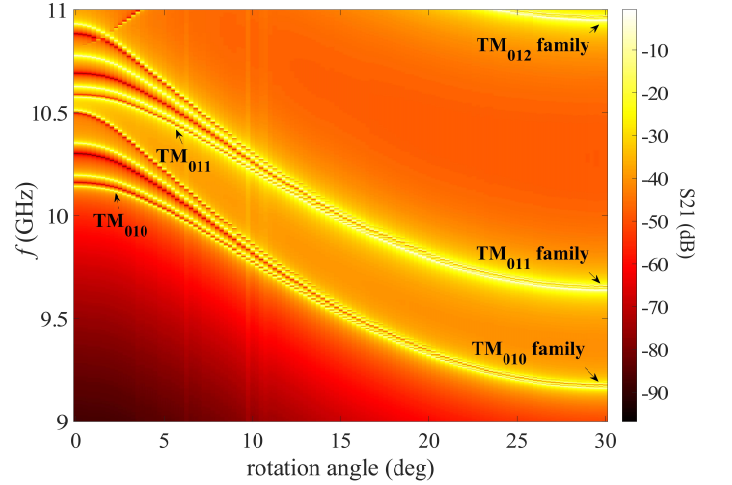


FIG. 4: Transmission S_{21} between two antennas on opposite endcaps as a function of tuning angle. A set of 121 driven modal simulations were performed setting copper conductivity at 4K as boundary condition. For the axion-sensitive TM_{010} mode the maximum frequency shift is about 1 GHz, with no mode mixings.

B. Study of allowed tolerances

resulting transmission spectra are shown in Fig. 4. The map shows two families of modes, each with four members that get closer at increasing tuning angles, which derive from the discretization of the TM_{010} and TM_{011} modes of the circular coaxial resonator. The lowest frequency modes in each family are those showing no zeros in the azimuthal direction. No mode crossings occur for the TM_{010} mode, which is always well-coupled with the antennas. In addition, we note that the separation between the modes exceeds their linewidths even for high tuning angles.

Complex cavity designs are more likely susceptible to deviations from the ideal geometry. We evaluate the required mechanical tolerances needed in this geometry by considering horizontal misalignment and tilts between the two prisms at $\phi = 0$. Fig. 5 reports the results for cavity parameters and figure of merit. We move the axis of the inner prism in the plane defined by the axis of the second prism and one of its vertexes. We separately study the effect of horizontal misalignment and of tilts about the center of the cavity.

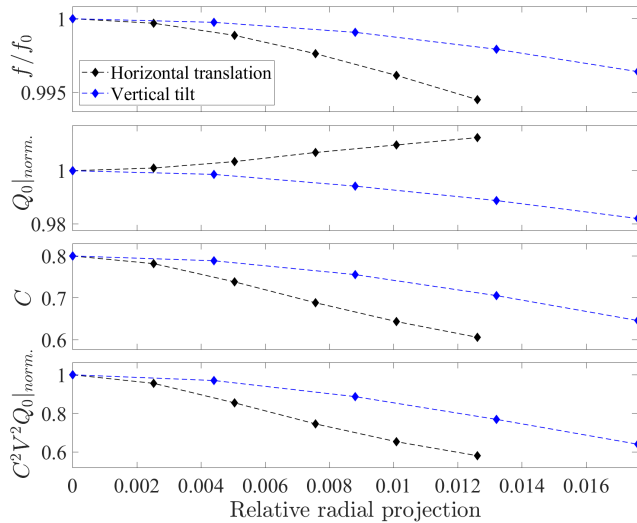


FIG. 5: Changes in the main cavity parameters due to varying degrees of reciprocal horizontal misalignment or tilting of the two prisms. In the case of the 10 GHz cavity, the endpoint of the blue curve corresponds to a lateral shift of $\sim 210 \mu\text{m}$. From top to bottom: relative frequency shift, normalized quality factor $Q_0|_{norm.}$, C factor and normalized figure of merit. Q_0 of the unperturbed cavity was 62000.

The two datasets are presented in the same plot where the horizontal axis is the relative radial projection, i.e. the displacement of the intercept of the inner prism axis with the top endcap, normalized to the prisms circumradius difference.

Horizontal misalignments significantly impact the C factor and thus are the main source of cavity figure of merit degradation. Quality factor and resonant frequency changes are much smaller. To limit the scan rate degradation due to horizontal translations within 10%, the minimum tolerance needed would be of about $75 \mu\text{m}$, within the capabilities of computerized numerical control machines.

III. EXPERIMENTAL RESULTS

A full-scale prototype of the cavity was obtained from bulk aluminium metal via single-pass wire electrodischarge machining (wire EDM) and is shown in Fig. 6. The 420 mm-long cavity has r_{in} and r_{ext} of 55.91 mm and 39.14 mm, respectively. The longitudinal edges of the inner and outer prism are filleted with radii of 2 mm and 3 mm, respectively. In this prototype, the endcaps are divided into two pieces through a $50 \mu\text{m}$ -wide circular gap, allowing for rotation of the inner prism via a knob. Each endcap hosts 8 apertures used for antenna insertion and dielectric bead pull characterization [38]. Of those, 6 were positioned in correspondence of the outer prism vertexes, while the other two were in the middle of a side.

All apertures were radially positioned to lay at the center of the cavity gap.

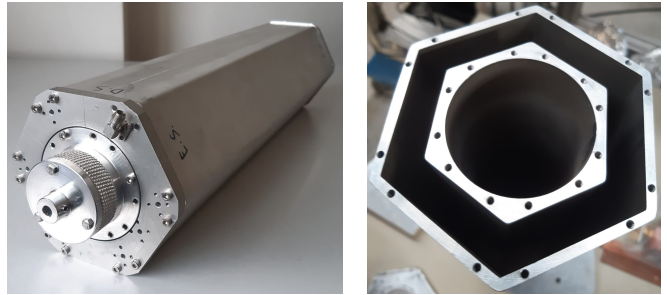


FIG. 6: The prototype hexagonal coaxial resonator. Left: external view. Right: internal view.

The measured transmission spectrum of the cavity at $\phi = 0$ is shown in Fig. 7. The TM_{010} and TM_{011} modes are well-isolated and the spectrum is clean before TM_{010} , in agreement with simulation results shown in Fig. 5.

The frequency of the TM_{010} mode measured at room temperature was 10.1855 GHz, to be compared with 10.14 GHz yielded from numerical simulations. The measured quality factor was ~ 4200 , with negligible couplings on both antennas. In the $\phi = 0$ configuration, the field profiles and transmission spectra were independent of antenna positioning. The full tuning range for a rotation from 0 to ϕ_{max} was about 1 GHz, as expected from simulations.

Measurements of field profiles evidenced the presence of geometrical nonidealities. Fig. 7 shows bead pull results for the main mode and the two most adjacent ones. The TM_{010} mode longitudinal field profile peaks before the cavity center, and its magnitude at the endcaps differs significantly. Marked asymmetries are also visible in the TM_{011} and TM_{012} modes. The cavity prototype is therefore longitudinally asymmetric. Concerning the azimuthal field distribution, we monitored the maximum field amplitudes for the TM_{010} mode, evidencing variations up to a factor 3. Numerical control machine measurements revealed deviations from design dimensions of up to a maximum of 0.14 mm. Minor geometry adjustments in the prism alignment resulted in a small frequency variation and no significant changes in the quality factor.

Subsequently the cavity was internally coated with copper tape strips, which improved the room temperature Q_0 to 9400, to be compared with the value of 10900 obtained for a bulk OHFC copper cavity from simulations. Cooling to 77 K improved Q_0 to 17800, smaller than the simulated value of 32900. Among the possible reasons for this discrepancy may be a lower than expected improvement in RF conductivity for the copper tape, or additional geometrical nonidealities in the prototype induced by thermal contractions.

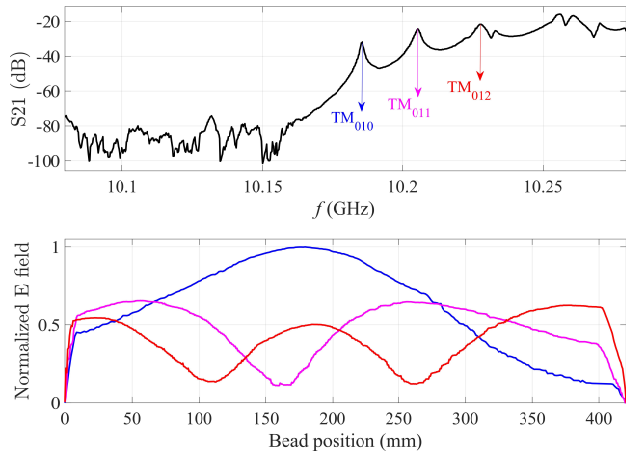


FIG. 7: Experimental results. The upper panel reports the transmission spectrum measured at $\phi = 0$, where we also indicate the position of the first three TM_{01n} modes. The corresponding measured electric field profiles are shown in the lower panel with the same colours.

IV. CAVITY COMPARISONS

In Fig. 8 we report the overall figure of merit F (see eq. 3) of the polygonal coaxial cavity for various magnet bore values. The working frequency has been set to 10 GHz and F is normalized to the value F_c obtained for a single cylindrical cavity of radius 11.48 mm resonating at the same frequency. For comparison, we also add the performances of some cavity setups described in the introduction: pizza cavities and cavity arrays. In the latter case, the normalized factor of merit is K and K^2 in the case of independent and coherent cavity arrays, respectively. The following assumptions have been made:

- the external wall thickness is 3 mm for all cavities;
- to fix TM_{010} at 10 GHz for the polygonal cavity, the gap thickness is kept constant for increasing magnet bore, while the number of sides is qualitatively scaled as the square root of the magnet bore. The external radius is adjusted to the maximum possible value. The C factor is 0.8 and we use a conservative value of 50000 for the quality factor;
- the data series for the pizza cavities are based on published data [24] obtained with 2, 4, 6 and 8 sections, rescaling the cavity dimensions to ensure resonance at 10 GHz. Their quality factors are respectively 68000, 62000, 55000, 50000 with $C = 0.65$;
- for the cavity arrays, we set cylindrical geometry with $Q_0 = 100000$ and $C=0.69$. The cavities are arranged to optimally fill the available volume. Arrays of 2 to 34 cavities can be hosted within the bore.

In Fig. 8, we identify three regions of interest for high frequency haloscopes. Below 80 mm-diameter magnet

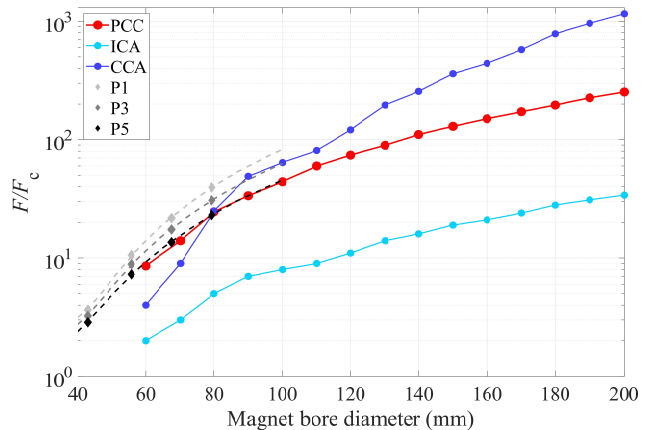


FIG. 8: Comparison between normalized figures of merit for different resonant cavity systems filling a magnet bore in a 10 GHz haloscope. PCC - polygonal coaxial cavity; ICA - independent cavity array; CCA - coherent cavity array. P1, P3 and P5 - pizza cavities employing diaphragms of 1, 3 and 5 mm thickness, respectively. The corresponding dashed lines are second order polynomial fits, while the solid lines only represent a guide to the eye.

bore, the pizza cavity is the best approach, as arrays of cylindrical cavities have low tessellation efficiency. The performance of the present polygonal coaxial cavity is comparable to a pizza cavity using 5 mm-thick diaphragms (P5 in Fig. 8). Between 80 and 120 mm the polygonal cavity approach is a competitive solution for its higher simplicity compared to pizza cavities with 10 to 16 subdivisions and arrays of 5 to 11 cavities. In principle, arrays of cylindrical cavities would give the best figure of merit for bore magnets greater than ~ 120 mm. However, one should be able to coherently readout a number of cavities ranging between 11 and 34, while the polygonal coaxial resonator is a practical solution. Moreover, multiple cavity arrays can be based also on nested polygonal coaxial cavities, greatly reducing the total number of cavities to be operated in parallel.

V. CONCLUSIONS

We introduced the tunable polygonal coaxial axion haloscope, and discussed it as a practical solution to the issue of the poor scaling of the scan rate with volume, particularly challenging in haloscopes in the range above ~ 5 GHz. Compared to arrays of cavities, and the pizza cavity concept, this resonator presents a significant figure of merit and allows for a practical and effective tuning method by relative rotation of the internal prism with up to 5% tuning depth.

FEM simulations were employed to study relevant cavity parameters over the tuning range. No mode mixings were observed. We also estimated the required mechanical tolerances, which were found to be within the capabil-

ities of commonly available numerical control machines.

A prototype aluminium hexagonal cavity was built and tested. The axion-sensitive mode was found near the expected frequency and was isolated for the full expected tuning range. Bead pull measurements were used to map the longitudinal field profiles and the azimuthal field distribution inside the resonator, showing unwanted asymmetries due to geometrical nonidealities of the prototype. More precise machining techniques, such as numerical control, will therefore be needed for future realizations. The cavity's inner surfaces were covered with copper tape strips to increase its quality factor. At room temperature, this allowed to reach $Q_0 \sim 10^4$, not far from the expected value. At liquid nitrogen temperature, the measured Q_0 of the coated cavity was short of the simulated value for reasons not yet completely understood. Most likely, this is due to a limited RF low temperature conductivity of the copper strips, or to variation of RF contact in the endcaps due to thermal contractions. The tuning mechanism should therefore be designed for cryogenic measurements, for instance including ball bearing guides. Flexible gaskets or quarter-lambda chokes should also be considered to ensure good RF connections.

In conclusion, the polygonal resonator represents an

effective 3D resonator for axion dark matter haloscope searches at high frequency. Much higher quality factors up to the range of millions could be reached by coating the internal walls with high temperature superconductor strips (see [39]). Additionally, even more efficient magnet bore occupation can be obtained by nested multiple polygonal coaxial cavities.

ACKNOWLEDGMENTS

This material was based upon work supported by INFN (QUAX experiment).

We are grateful to E. Berto (University of Padova and INFN) who substantially contributed to the mechanical realization of this cavity. A. Benato, A. Pitacco and M. Rebeschini of INFN Padova did part of the mechanical work and M. Zago (INFN) the mechanical drawings. The contribution of F. Calzaon and M. Tessaro (INFN) to the measurement set-up is gratefully acknowledged. The authors also thank A. Palmieri for useful discussions on the cavity concepts and M. Comunian for providing the server for FEM analysis.

-
- [1] S. Weinberg, A new light boson?, *Phys. Rev. Lett.* **40**, 223 (1978).
 - [2] F. Wilczek, Problem of strong p and t invariance in the presence of instantons, *Phys. Rev. Lett.* **40**, 279 (1978).
 - [3] R. D. Peccei and H. R. Quinn, CP conservation in the presence of pseudoparticles, *Phys. Rev. Lett.* **38**, 1440 (1977).
 - [4] R. D. Peccei and H. R. Quinn, Constraints imposed by CP conservation in the presence of pseudoparticles, *Phys. Rev. D* **16**, 1791 (1977).
 - [5] I. G. Irastorza and J. Redondo, New experimental approaches in the search for axion-like particles, *Progress in Particle and Nuclear Physics* **102**, 89 (2018).
 - [6] R. L. Workman and Others (Particle Data Group), Review of Particle Physics, *PTEP* **2022**, 083C01 (2022).
 - [7] M. Buschmann, J. W. Foster, A. Hook, A. Peterson, D. E. Willcox, W. Zhang, and B. R. Safdi, Dark matter from axion strings with adaptive mesh refinement, *Nature Commun.* **13**, 1049 (2022), arXiv:2108.05368 [hep-ph].
 - [8] P. Sikivie, Experimental tests of the "invisible" axion, *Phys. Rev. Lett.* **51**, 1415 (1983).
 - [9] D. Kim, J. Jeong, S. Youn, Y. Kim, and Y. K. Semertzidis, Revisiting the detection rate for axion haloscopes, *JCAP* **03**, 066, arXiv:2001.05605 [hep-ex].
 - [10] C. Bartram, T. Braine, R. Cervantes, N. Crisosto, N. Du, G. Leum, L. J. Rosenberg, G. Rybka, J. Yang, D. Bowering, A. S. Chou, R. Khatiwada, A. Sonnenschein, W. Wester, G. Carosi, N. Woollett, L. D. Duffy, M. Goryachev, B. McAllister, M. E. Tobar, C. Boutan, M. Jones, B. H. LaRoque, N. S. Oblath, M. S. Taubman, J. Clarke, A. Dove, A. Eddins, S. R. O'Kelley, S. Nawaz, I. Siddiqi, N. Stevenson, A. Agrawal, A. V. Dixit, J. R. Gleason, S. Jois, P. Sikivie, J. A. Solomon, N. S. Sullivan, D. B. Tanner, E. Lentz, E. J. Daw, M. G. Perry, J. H. Buckley, P. M. Harrington, E. A. Henriksen, and K. W. Murch (ADMX Collaboration), Axion dark matter experiment: Run 1b analysis details, *Phys. Rev. D* **103**, 032002 (2021).
 - [11] A. K. Yi, S. Ahn, i. m. c. b. u. Kutlu, J. Kim, B. R. Ko, B. I. Ivanov, H. Byun, A. F. van Loo, S. Park, J. Jeong, O. Kwon, Y. Nakamura, S. V. Uchaikin, J. Choi, S. Lee, M. Lee, Y. C. Shin, J. Kim, D. Lee, D. Ahn, S. Bae, J. Lee, Y. Kim, V. Gkika, K. W. Lee, S. Oh, T. Seong, D. Kim, W. Chung, A. Matlashov, S. Youn, and Y. K. Semertzidis, Axion dark matter search around 4.55 μeV with dine-fischler-srednicki-zhitnitskii sensitivity, *Phys. Rev. Lett.* **130**, 071002 (2023).
 - [12] I. Stern, A. A. Chisholm, J. Hoskins, P. Sikivie, N. S. Sullivan, D. B. Tanner, G. Carosi, and K. van Bibber, Cavity design for high-frequency axion dark matter detectors, *Rev. Sci. Instrum.* **86**, 123305 (2015), arXiv:1603.06990 [physics.ins-det].
 - [13] M. Simanovskaia, A. Droster, H. Jackson, I. Urdinaran, and K. van Bibber, A symmetric multi-rod tunable microwave cavity for a microwave cavity dark matter axion search, *Review of Scientific Instruments* **92**, 033305 (2021), https://pubs.aip.org/aip/rsi/article-pdf/doi/10.1063/5.0016125/13857698/033305_1_online.pdf.
 - [14] B. T. McAllister, G. Flower, L. E. Tobar, and M. E. Tobar, Tunable supermode dielectric resonators for axion dark-matter haloscopes, *Phys. Rev. Appl.* **9**, 014028 (2018).
 - [15] A. P. Quiskamp, B. T. McAllister, G. Rybka, and M. E. Tobar, Dielectric-boosted sensitivity to cylindrical azimuthally varying transverse-magnetic resonant modes in

- an axion haloscope, *Phys. Rev. Appl.* **14**, 044051 (2020).
- [16] J. Kim, S. Youn, J. Jeong, W. Chung, O. Kwon, and Y. K. Semertzidis, Exploiting higher-order resonant modes for axion haloscopes, *J. Phys. G* **47**, 035203 (2020), arXiv:1910.00793 [physics.ins-det].
- [17] D. Alesini *et al.* (QUAX), Realization of a high quality factor resonator with hollow dielectric cylinders for axion searches, *Nucl. Instrum. Meth. A* **985**, 164641 (2021), arXiv:2004.02754 [physics.ins-det].
- [18] R. Di Vora, D. Alesini, C. Braggio, G. Carugno, N. Crescini, D. D'Agostino, D. Di Gioacchino, P. Falferi, U. Gambardella, C. Gatti, G. Iannone, C. Ligi, A. Lombardi, G. Maccarrone, A. Ortolan, R. Pengo, A. Retaroli, G. Ruoso, L. Taffarello, and S. Tocci, High- q microwave dielectric resonator for axion dark-matter haloscopes, *Phys. Rev. Appl.* **17**, 054013 (2022).
- [19] D. Alesini *et al.* (QUAX), High quality factor photonic cavity for dark matter axion searches, *Rev. Sci. Instrum.* **91**, 094701 (2020), arXiv:2002.01816 [physics.ins-det].
- [20] S. Bae, S. Youn, and J. Jeong, Tunable photonic crystal haloscope for high-mass axion searches, *Phys. Rev. D* **107**, 015012 (2023).
- [21] Y. Kishimoto, Y. Suzuki, I. Ogawa, Y. Mori, and M. Yamashita, Development of a cavity with photonic crystal structure for axion searches, *PTEP* **2021**, 063H01 (2021), arXiv:2103.00101 [hep-ex].
- [22] M. Lawson, A. J. Millar, M. Pancaldi, E. Vitagliano, and F. Wilczek, Tunable axion plasma haloscopes, *Phys. Rev. Lett.* **123**, 141802 (2019).
- [23] A. J. Millar *et al.* (ALPHA), Searching for dark matter with plasma haloscopes, *Phys. Rev. D* **107**, 055013 (2023), arXiv:2210.00017 [hep-ph].
- [24] J. Jeong, S. Youn, S. Ahn, J. E. Kim, and Y. K. Semertzidis, Concept of multiple-cell cavity for axion dark matter search, *Phys. Lett. B* **777**, 412 (2018), arXiv:1710.06969 [astro-ph.IM].
- [25] J. Jeong, S. Youn, and J. E. Kim, Multiple-cell cavity design for high mass axion searches: An extended study, *Nucl. Instrum. Meth. A* **1053**, 168327 (2023), arXiv:2205.01319 [hep-ex].
- [26] A. Álvarez Melcón *et al.*, Scalable haloscopes for axion dark matter detection in the $30\mu\text{eV}$ range with RADES, *JHEP* **07**, 084, arXiv:2002.07639 [hep-ex].
- [27] C. Hagmann, P. Sikivie, N. Sullivan, D. B. Tanner, and S. Cho, Cavity design for a cosmic axion detector, *Review of Scientific Instruments* **61**, 1076 (1990), https://pubs.aip.org/aip/rsi/article-pdf/61/3/1076/19023464/1076_1_online.pdf.
- [28] D. S. Kinion, *First results from a multiple microwave cavity search for dark matter axions*, Other thesis (2001).
- [29] J. Yang, J. R. Gleason, S. Jois, I. Stern, P. Sikivie, N. S. Sullivan, and D. B. Tanner, Search for $5\text{--}9\ \mu\text{eV}$ Axions with ADMX Four-Cavity Array, *Springer Proc. Phys.* **245**, 53 (2020).
- [30] C. M. Adair *et al.*, Search for Dark Matter Axions with CAST-CAPP, *Nature Commun.* **13**, 6180 (2022), arXiv:2211.02902 [hep-ex].
- [31] J. Jeong, S. Youn, S. Ahn, C. Kang, and Y. K. Semertzidis, Phase-matching of multiple-cavity detectors for dark matter axion search, *Astroparticle Physics* **97**, 33 (2018).
- [32] D. S. Kinion, *First results from a multiple-microwave-cavity search for dark-matter axions* (University of California, Davis, 2001).
- [33] C.-L. Kuo, Large-Volume Centimeter-Wave Cavities for Axion Searches, *JCAP* **06**, 010, arXiv:1910.04156 [physics.ins-det].
- [34] C.-L. Kuo, Symmetrically Tuned Large-Volume Conic Shell-Cavities for Axion Searches, *JCAP* **02**, 018, arXiv:2010.04337 [physics.ins-det].
- [35] T. A. Dyson, C. L. Bartram, A. Davidson, J. B. Ezekiel, L. M. Futamura, T. Liu, and C.-L. Kuo, Demonstration of a high-volume tunable axion haloscope above 7 GHz, (2024), arXiv:2402.01060 [physics.ins-det].
- [36] R. Bradley, J. Clarke, D. Kinion, L. J. Rosenberg, K. van Bibber, S. Matsuki, M. Mück, and P. Sikivie, Microwave cavity searches for dark-matter axions, *Rev. Mod. Phys.* **75**, 777 (2003).
- [37] Nonetheless, provided each cell has its own tunable antenna, the present polygonal resonator becomes a cavity array in which the multiple cavities have $C \sim 0.6$, $Q \sim 60000$ and are all tuned together over a large range. In addition, for phase-matched readout, the cavity cells would only need an additional fine-tuning mechanism to compensate for small frequency differences between cells.
- [38] S. Som, S. Seth, A. Mandal, and S. Ghosh, Bead-pull measurement using phase-shift technique in multi-cell elliptical cavity, *Proceedings of IPAC* **280**, 2011 (2011).
- [39] D. Ahn, O. Kwon, W. Chung, W. Jang, D. Lee, J. Lee, S. W. Youn, H. Byun, D. Youm, and Y. K. Semertzidis, Biaxially textured $\text{yba}_2\text{cu}_3\text{o}_{7-x}$ microwave cavity in a high magnetic field for a dark-matter axion search, *Phys. Rev. Appl.* **17**, L061005 (2022).